HHS Public Access

Author manuscript

Nat Nanotechnol. Author manuscript; available in PMC 2016 May 18.

Published in final edited form as:

Nat Nanotechnol. 2016 January ; 11(1): 95–102. doi:10.1038/nnano.2015.238.

A multi-phase transitioning peptide hydrogel for suturing ultra-small vessels

Daniel J. Smith[1,2], **Gabriel A. Brat**[3], **Scott H. Medina**[1], **Dedi Tong**[3], **Yong Huang**[4], **Johanna Grahammer**[3], **Georg J. Furtmüller**[3], **Byoung Chol Oh**[3], **Katelyn J. Nagy-Smith**[1,2], **Piotr Walczak**[5], **Gerald Brandacher**[3], and **Joel P. Schneider.**[1,*]

[1]National Cancer Institute, Chemical Biology Laboratory, Frederick, MD 21702 USA

[2]Department of Chemistry and Biochemistry, University of Delaware, Newark, DE 19716 USA

[3]Johns Hopkins University School of Medicine, Department of Plastic and Reconstructive Surgery, Vascularized Composite Allotransplantation (VCA) Laboratory, Baltimore, Maryland 21287 USA

[4]Johns Hopkins University, Department of Electrical and Computer Engineering, Baltimore, Maryland 21218 USA

[5]Johns Hopkins University School of Medicine, Department of Radiology and Radiological Science, Baltimore, Maryland 21287 USA

Abstract

Many surgeries are complicated by the need to anastomose, or reconnect, micron-scale vessels. Although suturing remains the gold standard for anastomosing vessels, it is difficult to place sutures correctly through collapsed lumen, making the procedure prone to failure. Here, we report a multi-phase transitioning peptide hydrogel that can be injected into the lumen of vessels to facilitate suturing. The peptide, which contains a photocaged glutamic acid, forms a solid-like gel in a syringe and can be shear-thin delivered to the lumen of collapsed vessels (where it distends the vessel), and the space between two vessels (where it is used to approximate the vessel ends). Suturing is performed directly through the gel. Light is used to initiate the final gel-sol phase transition that disrupts the hydrogel network, allowing the gel to be removed and blood flow to resume. This gel adds a new tool to the armamentarium for micro- and supermicrosurgical procedures.

Graphical abstract

*Corresponding author, Tel: 301 846 5954, ; Email: schneiderjp@mail.nih.gov

Author contributions: D.J.S., G.A.B., G.B. and J.P.S. conceived the research. D.J.S., S.H.M. and K.J.N.-S. were responsible for the synthesis, biophysical and rheological characterization of materials. G.A.B., D.T., Y.H., J.G., G.J.F., B.C.O., P.W. and S.H.M. performed animal experiments. D.J.S., S.H.M., G.B. and J.P.S. wrote the manuscript.

Supplementary information accompanies this paper at www.nature.com/naturenanotechnology.

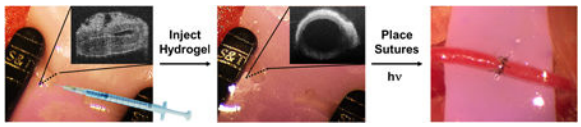

Microvascular anastomosis is critical in reconstructive surgery, especially for free tissue transfer, lymphaticovenous anastomosis and perforator flap surgery[1]. Although anastomosing 1-2 mm diameter vessels can be routinely accomplished by skilled surgeons, reconnecting micron-sized vessels is exceedingly difficult even for those who specialize in vascular- or microsurgery. The procedure is time-consuming, requires sophisticated instrumentation, and there is a steep learning curve for the training surgeon [2]. Procedures employing the anastomosis of micron-sized vessels are also critical in cardiac bypass, vascular, and pediatric transplant surgeries, as well as vascularized composite allotransplantation, and lymphatic supermicrosurgery. Optimal vascularization allows complex procedures to be performed that were previously unthinkable and considered technically impossible. In addition to impacting patient outcome, ultra-small anastomosis is critical in a multitude of research settings that employ animal models having small vasculature such as mice. Although assisting devices, such as couplers, clips, cuffs, lasers and various adhesives can facilitate the anastomosis of millimeter-sized vessels, they either do not support or have not been widely adopted for vessels having ultra-small features [3].

Suturing remains the gold standard for anastomosing ultra-small vessels [4], but has associated drawbacks of being difficult to accomplish and prone to failure [5,6]. Excessive handling of these vessels during their approximation can result in vessel weakening, intima damage, and increased risk of thrombosis. In addition, placing sutures correctly through the collapsed lumen, in particular in venous and lymphatic vessels of micron-sized diameters, is nearly impossible and misplaced sutures can lead to vessel stricture and decreased rates of patency. Despite these drawbacks, suturing is still one of the most widely used methods for anastomosing these delicate vessels. Thus, microsurgical aids that address the difficulties encountered with ultra-small vessel anastomosis should have tremendous impact in the clinic as well as the laboratory.

We report a peptide-based gel capable of multiple phase transitions that enable its use in greatly facilitating the anastomosis of ultra-small vessels. Self-assembled peptide gels are particularly attractive for this application since their mechanical properties can be tuned by precise design changes at the amino acid level. The gel described herein is formed from a self-assembling peptide whose initial sol-gel transition is directly triggered in a syringe. The resulting solid-like hydrogel can be shear-thin syringe delivered to the collapsed lumina of vessels where it re-establishes their shape, greatly aiding the suturing of the vessel (Figure 1a). The hydrogel can also be delivered to the inter-space between vessels where it can be used to approximate vessel ends via their insertion into the shear-thinning medium. This allows clamp-free approximation with minimal lumina handling. Sutures can be placed in a normal fashion directly through the gel medium. After suturing is complete, external gel is washed away and intravascular gel dissolved by initiating its final gel-sol phase transition via irradiation with light. In contrast to photoactivated bioadhesives whose treatment with

light induces gel formation [7,8], our design employs light to, instead, disassemble the material on completion of the surgical procedure.

Peptide Hydrogel Design and Rheological Properties

The peptide sequence of anastomosis photocaged 1 (APC1) contains seven lysine residues that are protonated at neutral pH, keeping the peptide soluble and in its monomeric unfolded state. As will be shown, a sol-gel phase transition can be initiated by triggering the folding of the peptide into an amphiphilic β-hairpin[9,10]. Once folded, APC1 is designed to rapidly self-assemble into a fibrillar hydrogel network, where each fibril is composed of a bilayer of β-hairpins that are intermolecularly hydrogen-bonded along the long-axis of a given fibril, Figure 1b (transition I) and 2b. Earlier studies in our lab support this proposed mechanism where the formation of the hydrophobic interface that defines the fibril bilayer provides most of the thermodynamic driving force for self-assembly[11–13].

We, and the Pochan laboratory, have shown that hydrogels formed from hairpin peptides display shear-thin/recovery rheological behavior[14–16]. When these gels experience a shear stress, such as that delivered by a syringe plunger, some of the interactions that stabilize their fibril network can be disrupted allowing the material to flow[17,18]. When the application of shear stress ceases, the network heals and the gel recovers (Figure 1b, transition ii). As will be shown, APC1 exhibits similar behavior, allowing its syringe-based delivery.

To induce the final gel-sol transition that allows the material within the sutured vessel to dissolve, we sought to disrupt the hydrogel network by destabilizing the hydrophobic interior of its fibrils, Figure 2b. APC1 incorporates a photocaged glutamic acid, namely 4-methoxy-7-nitroindolinyl glutamic acid [E(MNI)] on its valine-rich face, which would reside in the hydrophobic bilayer of the peptide fibril. When the gel is irradiated with 365 nm light, or alternatively through 2-photon irradiation at 720 nm, the cage is released introducing a negatively charged glutamate side chain into the hydrophobic bilayer, which is energetically unfavorable. This locally disruptive interaction is additive and should result in the global destabilization of the fibril network defining the gel state, thus initiating the final gel-sol transition (Figure 1b, transition iii and Figure 2a).

The MNI cage, chosen for its efficient aqueous photolysis and cytocompatibility [19,20], is incorporated at position 14 of APC1's primary sequence. This is a central position on the hairpin's hydrophobic face that corresponds to a fully buried site within the fibril bilayer. Incorporating the cage at this position necessitates the placement of a glycine residue on the opposing strand of the hairpin at position 7. In the self-assembled state, the small glycine provides a hole on the hydrophobic face of one folded hairpin into which the caged side chain from a neighboring hairpin can reside. This ‘lock and key’ side chain packing arrangement accommodates the large photocage within the tight steric constraints of the bilayer interior. Similar accommodations can be found in naturally occurring β-sheet proteins. For example, aryl residues can be found in sheet interiors with their aromatic side chains laying over a glycine residue in a neighboring strand [21]. The formation of favorable π-π interactions between the aromatic side chain and the glyl-amide backbone drives this fold [22]. Although the extended length and flexibility of the caged side chain could allow for

multiple modes of packing, molecular modeling shows that in the context of the APC1 hairpin, the proposed 'lock and key' arrangement results in a well-packed hydrophobic face that is conducive to bilayer formation (Figure 2b). Figure 2c shows a cut-away view of one monolayer formed from three hairpins. Here, the caged side chain from one hairpin lays over the glycine of a neighboring hairpin below it, with the indoline group making hydrophobic contacts with proximal valine side chains. The top-most hairpin in the assembly shown in panel c highlights the glycine hole into which a photocaged side chain could be placed if an additional hairpin were to join the fibril assembly.

In addition to APC1, a second peptide was designed to study the positional effect of cage placement on gel performance. Peptide APC2 contains the [E(MNI)] residue at position 16, which is slightly closer to the hairpin's C-terminus. Correspondingly, a glycine residue was incorporated at position 5. Two control peptides were also prepared, namely cAPC1 and cAPC2, which contain uncaged glutamate residues at positions 14 and 16, respectively.

The ability of APC1 and APC2 to fold and associate into β-sheet rich assemblies was monitored using circular dichroism (CD) spectroscopy. In water at 5 °C, the CD spectra of 1 wt% solutions of APC1 and APC2 indicate that the peptides are unfolded (Figure 3a). However, Figure 3b shows that folding and self-assembly can be triggered by adding pH 7.4 buffer that contains NaCl to the aqueous peptide solution and increasing the temperature to 25 °C for APC1 and to 37 °C for APC2. The NaCl screens the lysine point charges and increasing the temperature drives the hydrophobic effect, both of which favor folding and assembly. The exact temperatures needed to induce gelation was determined by monitoring the mean ellipticity at 216 nm as a function of temperature, Figure S3. In these CD experiments, self-supporting hydrogels of both peptides (pH 7.4, 150 mM NaCl) form directly in the cuvette. Spectra of both peptides in the gelled state display distinct minima at 216 nm, which is indicative of β– sheet secondary structure. Also evident in the spectra are absorptions due to the indoline cage, which occur in the near UV-CD (240-380 nm). These absorptions do not appear in the spectra of the unfolded peptides. This indicates that in the unfolded state of each peptide, the achiral aromatic indoline ring resides in an achiral environment, that is, it is solvent exposed. However, when the peptides fold and assemble, the ring is placed into a chiral environment, such as that provided by the fibril's hydrophobic interior. Importantly, under the same solution conditions that support APC1 and APC2 assembly, the control peptides cAPC1 and cAPC2 remain unfolded, Figure S4. This suggests that the control peptides' negatively charged glutamate side chains are not accommodated within the hydrophobic interior of the fibril bilayer and thus, peptide folding and assembly are disfavored. Importantly, it also supports the assertion that if the glutamate's negative point-charge were to be unmasked when the peptides are in the folded and assembled fibrillar state, that this event should be disruptive.

Oscillatory rheology was employed to study the rheological behavior of each gel under experimental conditions that mimic its use during the anastomosis procedure. Here, the storage modulus (G'), a measure of the gels' mechanical rigidity, is monitored in the rheometer under environmental conditions that mimic: (1) the initial (sol-gel) formation of the hydrogel in the syringe; (2) shear thinning of the material during injection with subsequent hydrogel recovery in the vessel lumen; and (3) the disruption of the gel network

(gel-sol) by UV photolysis after suturing. Monitoring gel behavior in a rheometer, although not exactly capturing the gel's response during the actual anastomosis procedure, allows quantitative and reproducible measurement of gel mechanical properties under highly controlled conditions. Figure 3c shows the data for APC1. In regime I, the rate of hydrogel formation (sol-gel) is assessed by monitoring the evolution of G' after peptide folding and assembly is triggered. APC1 forms a semi-rigid gel within the first few minutes that further rigidifies with time (G'~2,500 Pa after 30 minutes). After completion of the initial time sweep, 1000% strain is applied to the material for 30 seconds in regime II to mimic syringe delivery of the gel. This application of strain results in an immediate decrease in G' indicative of shear thinning that results in a viscous gel capable of flow. After the 30 seconds, the applied strain is decreased allowing the APC1 gel network to recover to about 75% (~1900 Pa) of its original rigidity. Lastly, using an optically clear parallel plate in the rheometer, the recovered hydrogel is subjected to irradiation by UV light (365 nm) for the first 10 minutes of regime III. The data clearly show that the gel network is rapidly degraded with an almost immediate decrease of G' to ~180 Pa. Taken together, the rheological data suggests that APC1 is capable of triggered gelation, shear-thin delivery via syringe and rapid post-delivery recovery. Importantly, irradiation by UV rapidly disrupts the gel network affording a viscous material, which should be capable of dissolution when exposed to the shear of blood flow.

Figure 3d shows the same experiment for the APC2 gel, where a significant lag phase before the onset of gelation is observed. However, with time, APC2 forms a gel that is significantly more stiff (20,000 Pa) then that formed from APC1. In regime II, the APC2 gel shear thins but is unable to self-heal effectively and recovers only about 5% of its original mechanical rigidity. Irradiation in regime III disrupts the weakly recovered gel. Although APC2 initially forms a rigid gel, its inability to recover after being shear thinned precludes it use in the anastomosis procedure. Overall, this rheological data indicates that the positional placement of the photocage within the peptides' primary sequence is important. Here, incorporation of the cage near the hairpin's terminus hampers the ability of its network to recover. Based on this rheological assessment, the APC1 gel was chosen for further study.

Photolysis and its Effect on Fibril Network Morphology

The rheological data shows that irradiation of the recovered APC1 gel leads to a significant decrease in G′ presumably as a result of releasing the glutamate cage. This was confirmed by following the fate of caged APC1 during photolysis by UV spectroscopy and LCMS, which showed nearly complete release of the MNI cage and evolution of corresponding carboxylate-containing peptide within 90 seconds of irradiation, Figure S8. In Figure 4, transmission electron microscopy (TEM) shows the morphology of fibrils isolated from a 1 wt% APC1 hydrogel before (a) and after (b) irradiation. Before irradiation, the hydrogel network is composed of long fibrils whose lengths are distributed over a range of 150 nm to over 1000 nm, Figure 4c. Irradiation results in the formation of small fibril segments as shown in panels (b) and (d). The average length of these fibrils is on the order of ~ 150 nm demonstrating that the majority of longer fibrils have been converted to smaller segments as a result of photolysis. Further, CD spectroscopy of the irradiated gel shows an attenuation of β-sheet signal at 216 nm, which is consistent with the disruption of the fibril network, Figure

S9. The fact that some small fibrils persist may be due to either incomplete release of the cage, or that a population of the uncaged peptide remains in the fibrillar state. At any rate, the rheological data demonstrates, and as will be confirmed in the in vivo studies, this level of fibril disruption is sufficient to ensure the necessary gel-sol phase transition.

APC1 Hydrogel Facilitates Microvascular Anastomosis

The ability of the APC1 hydrogel to serve as a temporary aid in the suturing process was assessed in a mouse femoral artery end-to-end anastomosis model. This challenging microsurgical setting tests the gel with regards to ease, safety, precision, and speed of arterial anastomosis. The mouse femoral artery is approximately 200 microns in diameter and, conventionally, is anastomosed via a technically challenging and time-consuming "no-touch" under-water suturing technique. In contrast, the APC1 hydrogel is designed for facile administration directly to the in situ vessel to distend the lumen and add stability to the vessel wall. This should enable more precise and quick placement of stitches, resulting in increased vessel patency.

In this model, an incision is made in the groin crease of mice to expose the femoral artery, which is dissected and subsequently clamped, Figure 5a. Optical coherence tomography (OCT) [23] of the vessel cross-section shows that the lumen is collapsed, Figure 5b. Without the aid of a stent or luminal filler, the anastomosis of this vessel would be extremely difficult. An intraluminal injection of a 2 wt% APC1 hydrogel was administered by syringe to both severed ends of the vessel, distending the lumen (Figure 5c) and mechanically supporting the vessel wall after injection, Figure 5d. A longitudinal cross-section OCT image of the proximal (left) and distal (right) ends of the vessels after injection with the APC1 hydrogel is shown in Figure 5e. Vascular distention caused by the gel helped maintain a cylindrical vessel shape, facilitating identification of a single vessel wall leading to more uniform suture spacing and closure. Further, hydrogel can be applied between the vessels, aiding their approximation (see video S1). Vessel ends can be inserted into the gel, where local thinning occurs proximal to the vessels during their movement within the gel. Once the vessels are approximated, the gel instantaneously recovers, gently fixing them. This allows optimal placement of the vessel ends for suture placement. The needle can be passed directly through the optically clear gel to place the sutures. Upon placement of the final suture, the external gel is washed away, and the vessel is irradiated at the suture site for 2 minutes using a hand-held 365 nm LED UV light to remove the interior gel. Resumption of blood flow after removing the clamps clears the disrupted gel as evidenced by Volume Doppler OCT (Figure 5f) and blood flow speed measurements [24], Figure S10. Visual conformation of blood flow is also clearly shown in Figure 5g.

The efficacy of the final gel-sol phase transition is critical since remaining solid material could lead to thrombus formation, diminished perfusion and tissue ischemia. Thus, vessel patency was assessed in a series of experiments that monitor vascular perfusion. First, high-resolution micro-CT was used to follow the perfusion of a polymeric contrast agent (microfil) one hour after gel-based end-to-end anastomosis of the femoral artery and resumption of blood flow. Figure 6a-c and video S2 show that polymer completely fills the distal tibial and fibular vessels as well as the plantar arch on the footpad and the digital

branches to the toes. Separate experiments in which animals were dissected to directly observe polymer distribution support the CT data (Figure 6d-f), confirming occlusion free vascular patency throughout the entire extremity that is similar to the contralateral control limb. Lastly, perfusion of a near-infrared dye was followed throughout an explanted hind limb after irradiating a gel that had been implanted into the femoral artery, Figure 6g-i. The leading edge of the dye (green arrow) immediately penetrates the limb from its initial injection site (yellow arrow), quickly penetrating another major vessel (white arrow, h) and distant vascular regions and surrounding tissue (i). Taken together, these experiments indicate that the peripheral vascular and capillary bed is well perfused without any evidence of luminal narrowing or occlusion due to gel remnants. We also investigated gel biocompatibility, where histology shows a similar peri-vascular inflammatory response in vessels anastomosed with or without gel, a result of surgical tissue traumatization and post-operative healing, Figure S11. Further, subcutaneously injected gel produced no gross local inflammation and a typical foreign-body response that resolved, Figure S12.

Conclusions

Designing soft materials from self-assembling peptides allows their bulk properties to be engineered at the molecular level for specific applications. Physical attributes endeared to the peptide monomer are translated to the properties of the self-assembled gel network. The multiple phase transitions of APC1, which enable its use in facilitating the anastomosis of ultra-small vessels, are due to the exact placement of natural and non-natural amino acids within its sequence that render the peptide, and its corresponding gel, responsive to environmental change. Thus, *de novo* peptide design can afford a self-assembled material that represents a promising alternative to currently available non-injectable stents.

Methods

General methods describing the synthesis and analytical characterization of the photocaged glutamic acid and all peptides, as well as detailed procedures for all of the experiments employed in this study (including the number of animals used and replicates) can be found in the Supplementary Information in the online version of the paper. The supplementary information also contains AFM, additional rheological studies, histological analysis, and videos showing the gel-aided anastomosis and three-dimensional reconstruction of hind-limb vasculature.

Supplementary Material

Refer to Web version on PubMed Central for supplementary material.

Acknowledgments

This research was supported by the Intramural Research Program of the NIH, National Cancer Institute, Center for Cancer Research. We thank Brian Bush for performing the AFM analysis.

References

1. Gardiner MD, Nanchahal J. Strategies to ensure success of microvascular free tissue transfer. J Plastic Reconst Aesth Surg. 2010; 63:E665.
2. MacDonald JD. Learning to perform microvascular anastomosis. Skull Base - an Interdisciplinary Approach. 2005; 15:229.
3. Pratt GF, et al. Technology-assisted and sutureless microvascular anastomoses: Evidence for current techniques. Microsurgery. 2012; 32:68. [PubMed: 22121054]
4. Alghoul MS, et al. From simple interrupted to complex spiral: A systematic review of various suture techniques for microvascular anastamoses. Microsurgery. 2011; 31:72. [PubMed: 21207502]
5. Bui DT, et al. Free flap reexploration: Indications, treatment, and outcomes in 1193 free flaps. Plast Reconstr Surg. 2007; 119:2092. [PubMed: 17519706]
6. Disa JJ, Cordeiro PG, Hidalgo DA. Efficacy of conventional monitoring techniques in free tissue transfer: An 11-year experience in 750 consecutive cases. Plast Reconstr Surg. 1999; 104:97. [PubMed: 10597680]
7. Nakayama Y, Matsuda T. Photocurable surgical tissue adhesive glues composed of photoreactive gelatin and poly(ethylene glycol) diacrylate. J Biomed Mater Res. 1999; 48:511. [PubMed: 10421695]
8. Rickett TA, et al. Rapidly photo-cross-linkable chitosan hydrogel for peripheral neurosurgeries. Biomacromol. 2011; 12:57.
9. Schneider JP, et al. Responsive hydrogels from the intramolecular folding and self-assembly of a designed peptide. J Am Chem Soc. 2002; 124:15030. [PubMed: 12475347]
10. Nagy KJ, Giano MC, Jin A, Pochan DJ, Schneider JP. Enhanced mechanical rigidity of hydrogels formed from enantiomeric peptide assemblies. J Am Chem Soc. 2011; 133:14975. [PubMed: 21863803]
11. Haines-Butterick L, et al. Controlling hydrogelation kinetics by peptide design for three-dimensional encapsulation and injectable delivery of cells. Proc Nat Acad Sci USA. 2007; 104:7791. [PubMed: 17470802]
12. Pochan DJ, et al. Thermally reversible hydrogels via intramolecular folding and consequent self-assembly of a de Novo designed peptide. J Am Chem Soc. 2003; 125:11802. [PubMed: 14505386]
13. Rajagopal K, Ozbas B, Pochan DJ, Schneider JP. Probing the importance of lateral hydrophobic association in self-assembling peptide hydrogelators. Eur Biophys J. 2006; 35:162. [PubMed: 16283291]
14. Branco MC, Pochan DJ, Wagner NJ, Schneider JP. The effect of protein structure on their controlled release from an injectable peptide hydrogel. Biomaterials. 2010; 31:9527. [PubMed: 20952055]
15. Salick DA, Pochan DJ, Schneider JP. Design of an injectable beta-hairpin peptide hydrogel that kills methicillin-resistant staphylococcus aureus. Adv Mater. 2009; 21:4120.
16. Sinthuvanich C, Haines-Butterick LA, Nagy KJ, Schneider JP. Iterative design of peptide-based hydrogels and the effect of network electrostatics on primary chondrocyte behavior. Biomaterials. 2012; 33:7478. [PubMed: 22841922]
17. Rughani RV, Branco MC, Pochan DJ, Schneider JP. De novo design of a shear-thin recoverable peptide-based hydrogel capable of intrafibrillar photopolymerization. Macromol. 2010; 43:7924.
18. Yan CQ, et al. Injectable solid hydrogel: mechanism of shear-thinning and immediate recovery of injectable beta-hairpin peptide hydrogels. Soft Matter. 2010; 6:5143. [PubMed: 21566690]
19. Canepari M, Nelson L, Papageorgiou G, Corrie JET, Ogden D. Photochemical and pharmacological evaluation of 7-nitroindolinyl-and 4-methoxy-7-nitroindolinyl-amino acids as novel, fast caged neurotransmitters. J Neurosci Meth. 2001; 112:29.
20. Matsuzaki M, et al. Dendritic spine geometry is critical for AMPA receptor expression in hippocampal CA1 pyramidal neurons. Nature Neurosci. 2001; 4:1086. [PubMed: 11687814]
21. Hutchinson EG, Sessions RB, Thornton JM, Woolfson DN. Determinants of strand register in antiparallel beta-sheets of proteins. Protein Sci. 1998; 7:2287. [PubMed: 9827995]

22. Wouters MA, Curmi PMG. An analysis of side chain interactions and pair correlations within antiparallel beta-sheets - The differences between backbone hydrogen-bonded and non-hydrogen-bonded residue pairs. Prot Struct Funct Genet. 1995; 22:119.

23. Huang Y, et al. Microvascular anastomosis guidance and evaluation using real-time three-dimensional Fourier-domain Doppler optical coherence tomography. J Biomed Opt. 2013; 18

24. Huang Y, et al. Evaluation of microvascular anastomosis using real-time, ultra-high-resolution, Fourier Domain Doppler Optical Coherence Tomography. Plast Reconstr Surg. 2015; 135:711E.

25. Zuman P, Shah B. Addition, reduction, and oxidation reactions of nitrosobenzene. Chem Rev. 1994; 94:1621.

26. Papageorgiou G, Ogden D, Corrie JET. An antenna-sensitized nitroindoline precursor to enable photorelease of L-glutamate in high concentrations. J Org Chem. 2004; 69:7228. [PubMed: 15471473]

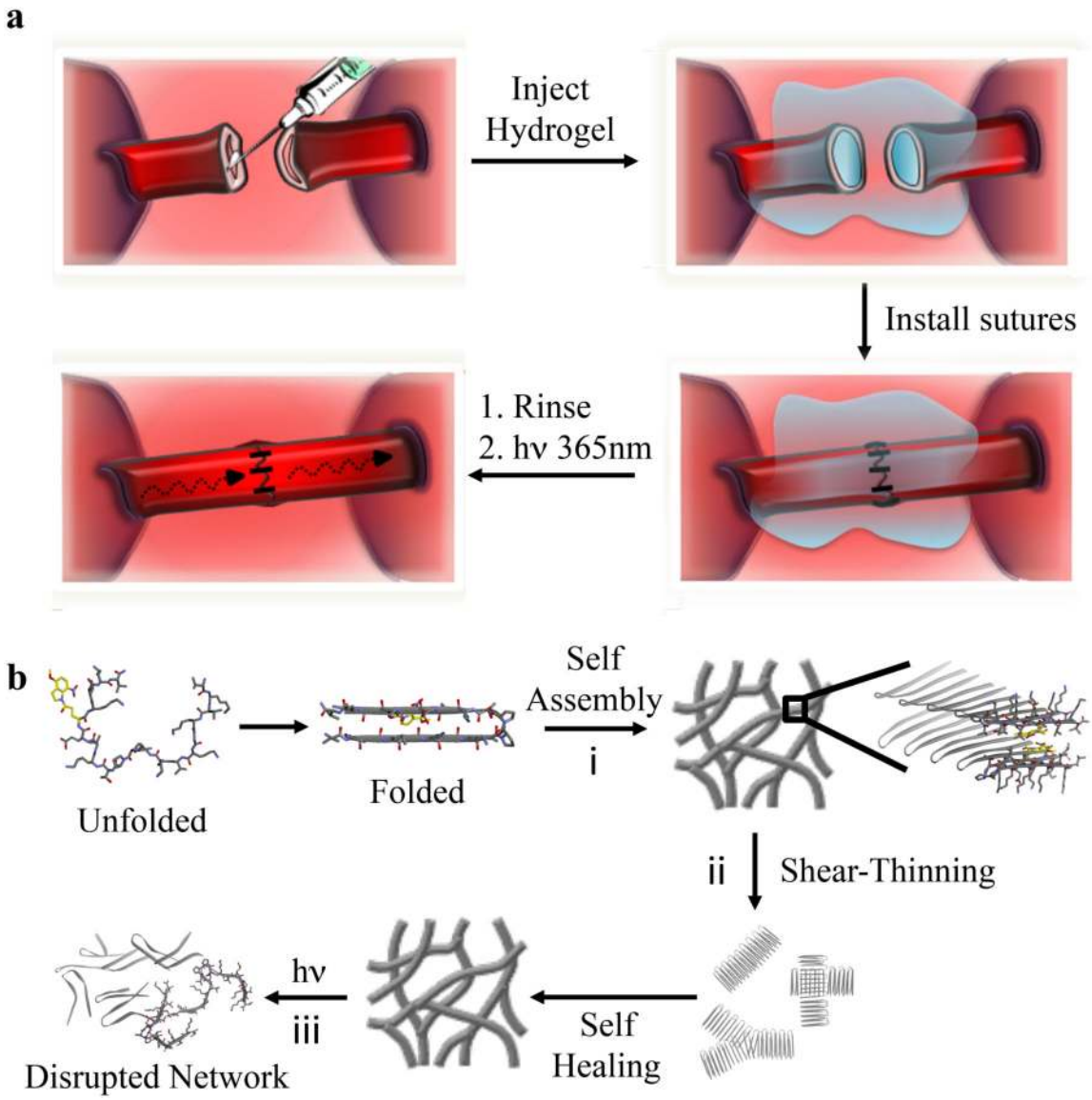

Figure 1. Conceptual design of the peptide hydrogel and its use in light-mediated suturing of ultra-small vessels

(a) Hydrogel formed directly in syringe by a triggered sol-gel phase transition is shear-thin/recovery injected into a collapsed vessel resulting in vascular distention, which greatly facilitates suturing. UV photolysis triggers the final gel-sol transition to allow blood flow. (b) Multiple phase transitions of APC1. (i) Triggered peptide folding and self-assembly leads to the formation of a fibrillar hydrogel network. (ii) Shear-thinning converts the solid-like gel to a viscous gel capable of flow. Cessation of applied shear allows gel recovery. (iii) Irradiation with UV destabilizes the fibril network and triggers the final gel-sol phase transition.

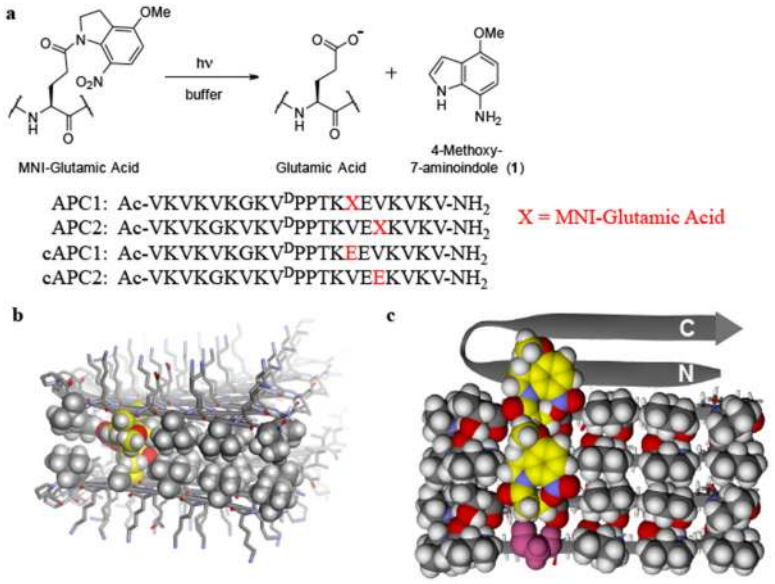

Figure 2. Molecular design of photosensitive APC1 gel

(a) Photolysis reaction of (MNI-Glu) producing glutamate and aminoindole byproduct **1** via reduction of the initially formed nitrosoindole [25]. Sequences of photocaged peptides (APC1, APC2) and the corresponding non-caged controls (cAPC1, cAPC2) are shown. (b) Energy minimized model showing the cross-section of a fibril formed by self-assembling APC1 β-hairpins. Peptides assemble laterally via hydrogen bonding to form the long axis of the fibril, which projects into the page. The amphiphilic hairpins also assemble facially, where the hydrophobic faces of each hairpin (shown by CPK space fill rendering) associate to form a bilayer that defines the hydrophobic interior of the fibril. Two caged glutamates (yellow) from distinct hairpins oppose each other across the bilayer. The exterior of the fibril is composed of polar amino acid side chains (stick figures) projected from the hydrophilic face of each hairpin in the assembly. Peptide backbones are displayed as ribbons; gray (carbon), white (hydrogen), blue (nitrogen), red (oxygen). (c) Bottom peptide monolayer, derived conceptually by removing its top partner monolayer in panel (b), viewed axially from above (only three hairpins are shown for clarity). The N- and C-termini for one hairpin ribbon is shown to orient the reader. Carbon atoms of each photocage are shown in yellow, highlighting their ‘lock and key’ packing arrangement. Starting from the bottom of the figure, the photocage of the first hairpin packs into a hole provided by a small glycine residue of the neighboring hairpin, which in turn, uses its cage to pack into its neighbor. The glycine residue of the bottom hairpin is shown in pink and highlights the region where the cage of an adjacent hairpin could pack if present. The photocage of the top-most ribbon hairpin is omitted for clarity. All colors are defined as in panel (b). Peptides were prepared by Fmoc-based solid phase peptide synthesis (Figures S1 and S2) employing Fmoc-protected [E(MNI)], which was synthesized using a modified literature procedure [26] as outlined in the Supplementary Information.

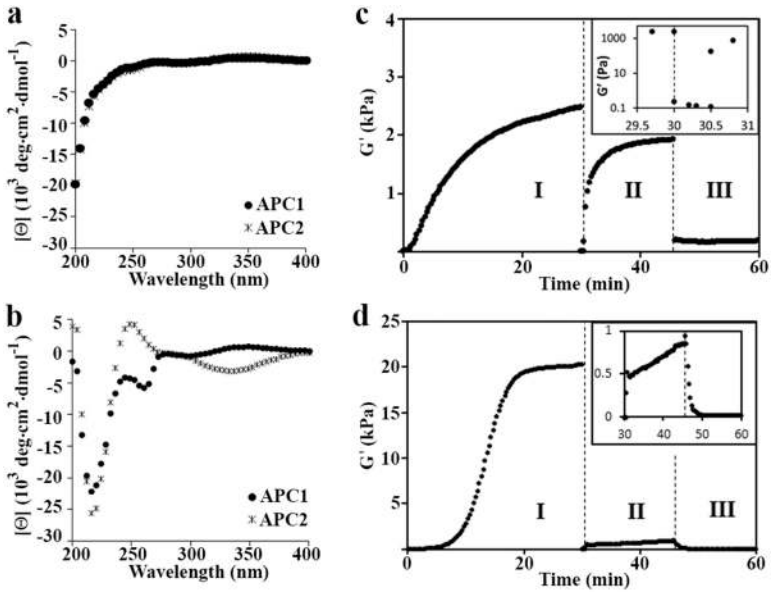

Figure 3. Biophysical and mechanical characterization of the hydrogel

(a) CD wavelength spectra of 1 wt% APC1 and APC2 in water at 5 °C showing that the peptides are unfolded. (b) Wavelength spectra of 1 wt% APC1 and APC2 hydrogels formed at pH 7.4 (150 mM NaCl) and 25 and 37 °C, respectively, indicating peptide folding and assembly. (c) Rheological assessment showing the formation, shear-thin/recovery and photodisruption of APC1 and (d) APC2 gels. In regime I, a dynamic time sweep monitors the initial sol-to-gel phase transition of each 1 wt% gel after folding and assembly is triggered by measuring the storage modulus (G') as a function of time at pH 7.4 and 37 °C for APC1 and 25 °C for APC2; frequency = 6 rad/s, 0.2% strain. In regime II, 1000% strain is applied for 30 seconds to thin the materials after which the strain is decreased to 0.2% to allow material recovery. Inset in panel (c) shows regimes I and II expanded, highlighting the gel-sol and subsequent sol-gel transitions. In regime III, the recovered gels are irradiated at 365 nm for 10 minutes to initiate the final gel-sol transition; G' is monitored during and after irradiation. Inset in panel (d) shows regimes II and III expanded. Independent frequency- and strain-sweep measurements (Figures S5 and S6), additional rheology experiments on pre-formed gels (Figure S7), and AFM measurements (Table S1) further support this rheological profile.

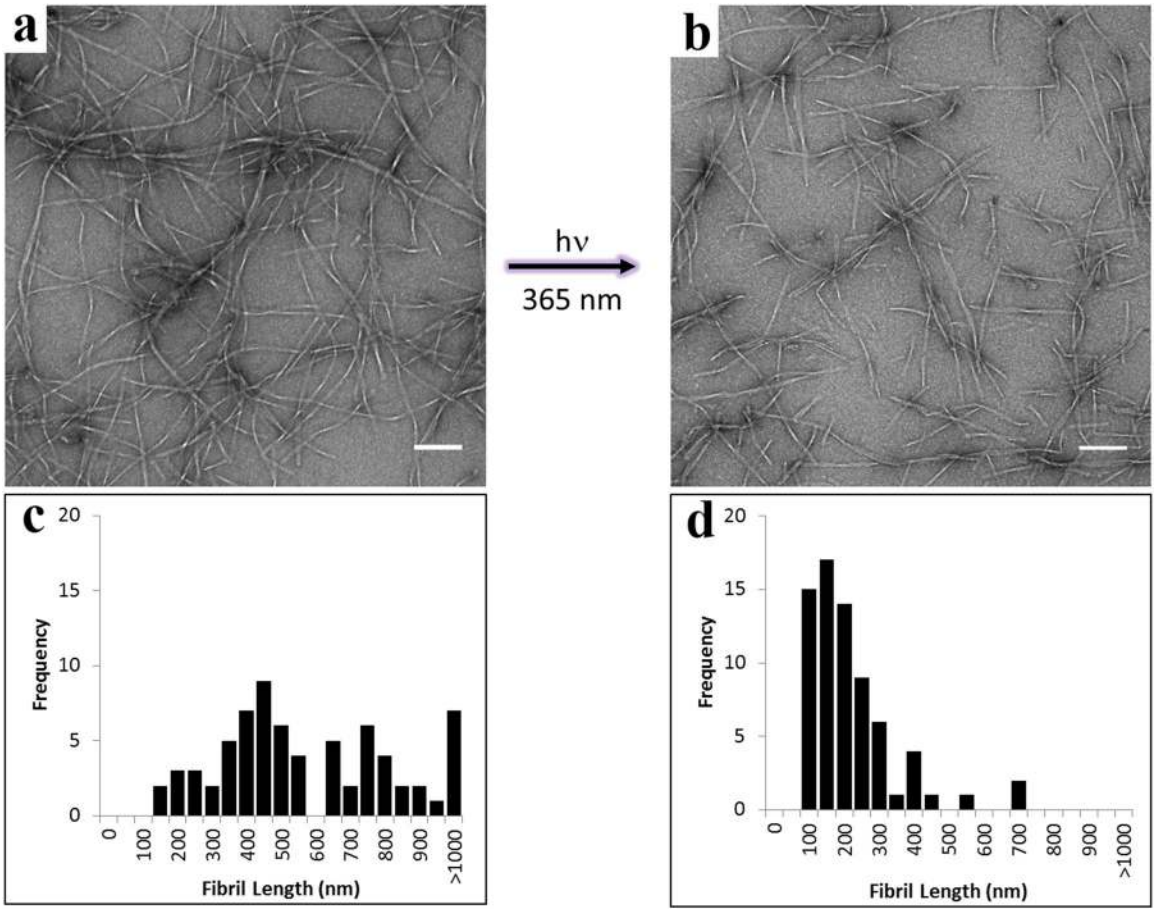

Figure 4. Fibril morphology as a function of photolysis

TEM analysis of fibrils isolated from a 1 wt% APC1 hydrogel (a) before and (b) after photolysis, indicating hydrogel network disruption. Scale bar = 100 nm. Distribution of measured lengths of fibrils from a 1 wt% APC1 gel (c) before and (d) after photolysis, n = 70 for both panels.

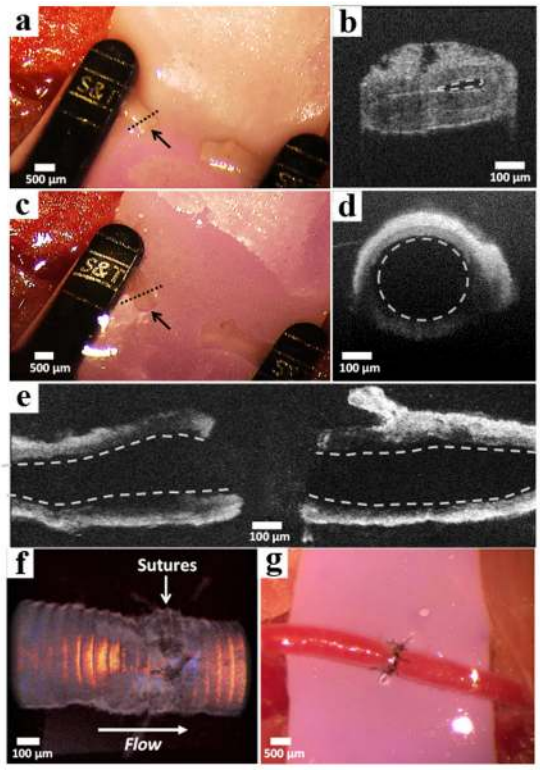

Figure 5. Assessment of vessel patency before and after gel-based anastomosis

(a) Collapsed femoral artery of a mouse indicated by the black arrow. (b) Optical coherence tomography (OCT) of the severed vessel cross-section. Collapsed vessel lumen indicated by the dashed line. The image was collected at the region of the vessel indicated by the dashed line in panel a. (c) Distended end with open lumen of artery after injection of 2 wt% APC1 hydrogel indicated by the black arrow. (d) OCT of the vessel cross-section showing the distended lumen (dashed circle). The vessel was imaged at the region indicated by the dashed line in panel c. (e) Horizontal cross-section of the proximal (left) and distal (right) vessel walls showing open lumina (dashed lines) after hydrogel injection. (f) OCT volume Doppler depiction of anastomosed artery after irradiation where the red, orange, and yellow regions indicate uncompromised blood flow through the suture site. (g) Macroscopic appearance of anastomosed femoral artery with normal blood flow.

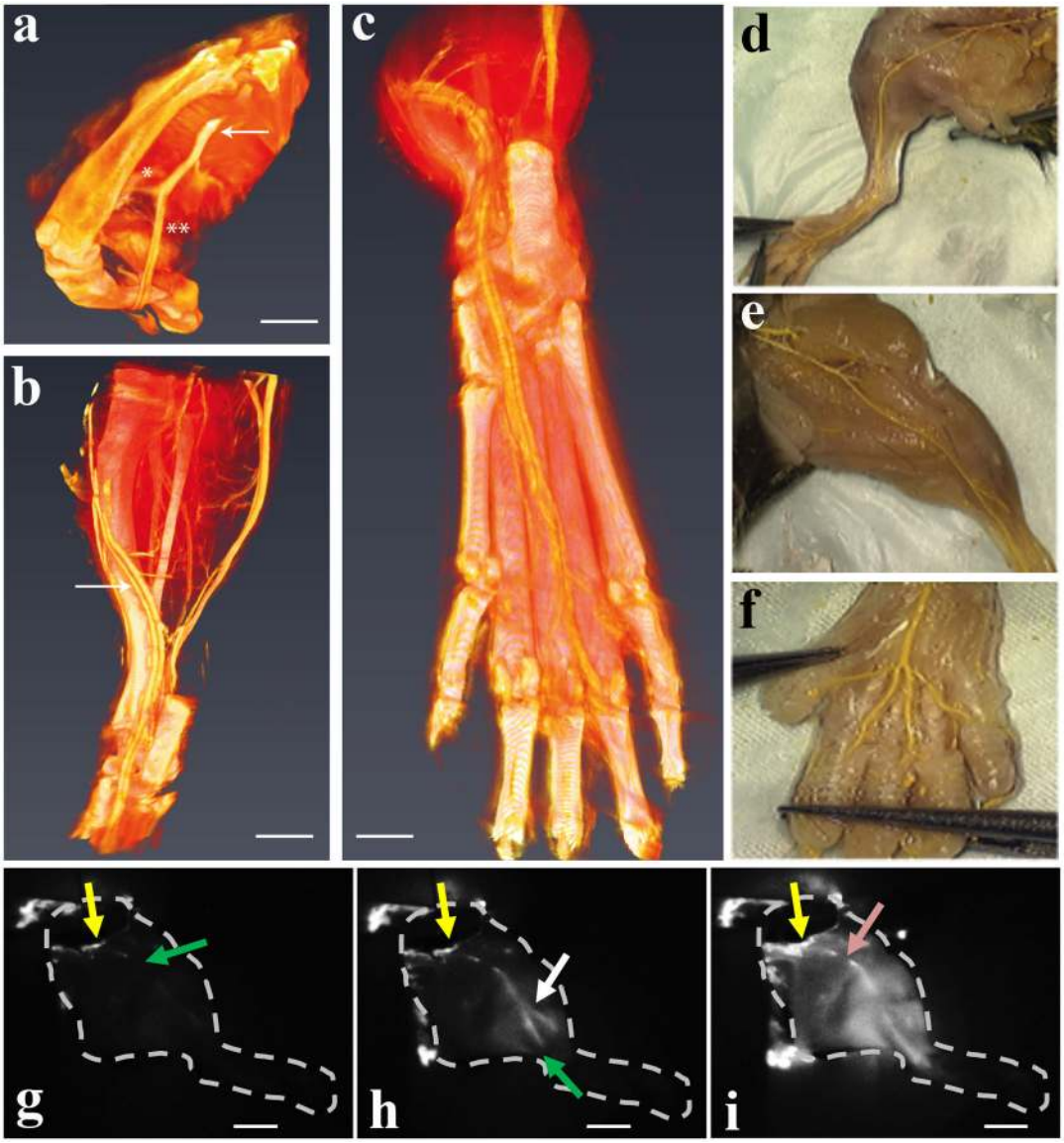

Figure 6. Perfusion of mouse lower limb after hydrogel supported end-to-end anastomosis of the femoral artery

(a) Micro-CT 3D rendering showing contrast agent perfusion through the anastomosed site including the distal femoral artery (arrow) and its bifurcation into the fibular [*] and tibial artery [**] (scale bar = 2.5 mm). Panel (b) depicts the tibial artery (arrow) in its anatomical course within the lower leg and ankle area (scale bar = 2.0 mm). Panel (c) illustrates the most distal aspects of tibial blood supply to the footpad and individual toes (scale bar = 0.5 mm). Panel (d) depicts a dissected anastomosed limb after polymer (yellow) diffusion. (e) shows the contralateral non-anastomosed control limb. (f) shows polymer perfusion to individual toes. Panels (g-i) follows the real-time perfusion of indocyanine green (ICG) dye through the vasculature of an explanted mouse hind limb after irradiation of an implanted APC1 hydrogel. Distribution of ICG, 2 seconds (g), 7 seconds (h), and 33 seconds (i) after injection. The arrows indicate the initial site of injection (yellow), the most distal location of the dye from the injection site (green), the perfusion through another major vessel (white),

and a minor obstruction (pink) that did not affect perfusion. Scale bars in panels (g-i) are 4 mm.